

Analysis of a crater-forming meteorite impact in Peru

P. Brown,¹ D. O. ReVelle,² E. A. Silber,¹ W. N. Edwards,³ S. Arrowsmith,²
L. E. Jackson Jr.,⁴ G. Tancredi,⁵ and D. Eaton⁶

Received 5 February 2008; revised 27 April 2008; accepted 3 June 2008; published 16 September 2008.

[1] The fireball producing a crater-forming meteorite fall near Carancas, Peru, on 15 September 2007 has been analyzed using eyewitness, seismic, and infrasound records. The meteorite impact, which produced a crater of 13.5 m diameter, is found to have released of order 10^{10} J of energy, equivalent to $\sim 2\text{--}3$ tons of TNT high explosives based on infrasonic measurements. Our best fit trajectory solution places the fireball radiant at an azimuth of 82° relative to the crater, with an entry angle from the horizontal of 63° . From entry modeling and infrasonic energetics constraints, we find an initial energy for the fireball to be in the 0.06–0.32 kton TNT equivalent. The initial velocity for the meteoroid is restricted to be below 17 km/s from orbit considerations alone, while modeling suggests an even lower best fit velocity close to 12 km/s. The initial mass of the meteoroid is in the range of 3–9 tons. At impact, modeling suggests a final end mass of order a few metric tons and impact velocity in the 1.5–4 km/s range. We suggest that the formation of such a substantial crater from a chondritic mass was the result of the unusually high strength (and corresponding low degree of fragmentation in the atmosphere) of the meteoritic body. Additionally, the high altitude of the impact site (3800 m.a.s.l) resulted in an almost one order of magnitude higher impact speed than would have been the case for the same body impacting close to sea level.

Citation: Brown, P., D. O. ReVelle, E. A. Silber, W. N. Edwards, S. Arrowsmith, L. E. Jackson Jr., G. Tancredi, and D. Eaton (2008), Analysis of a crater-forming meteorite impact in Peru, *J. Geophys. Res.*, 113, E09007, doi:10.1029/2008JE003105.

1. Introduction

[2] The fall of a meteorite to Earth is usually accompanied by a range of associated phenomena. These include the light produced from the accompanying fireball, ionization along the meteoroid atmospheric path and sound which may be audible at the Earth's surface. In some instances impact effects near the point of fall may also occur. Most commonly these include witnesses hearing the subsonic motion of large fragments [cf. Brown *et al.*, 1996] and/or noting directly the fall of fragments and production of plunge pits in the case of larger fragments. Very rarely fragments may impact with a substantial remnant of their pre-atmospheric velocity and produce penetration craters [French, 1989]. These craters are usually a few meters to a few tens of meters in diameter. In these instances, the cratering physics

is dominated by the exchange of momentum between the ground and impacting fragment, as opposed to being explosive/shock excavated as is the case for larger impacts. Small terrestrial impacts are often strength-dominated, meaning the target material plays a substantial role in determining the final crater characteristics, as opposed to larger craters which are typically gravity dominated and the target material is less important.

[3] Recent examples of penetration crater production include the Sikhote-Alin iron shower of 1947 [Krinov, 1966], the Jilin chondrite meteorite fall in 1976 [Joint Investigation Group, 1977], the Sterlitamak iron in 1990 [Petaev *et al.*, 1991] and most recently the Kunva-Urgench chondrite fall in 1998 [Mukhamednazarov, 1999]. In the case of the chondritic falls, the resulting penetration craters were only slightly larger than the impacting mass, while the iron impactors produced craters much larger than the impacting bodies. These cratering events are of interest as they provide insight into the mechanics of small crater production at the lower end of hypersonic speeds in the strength dominated regime on the Earth. Such impacts are relevant to cratering on some asteroids [cf. Holsapple, 1993] as inter asteroid velocities tend to be in the range of a few km/s and are also strength-dominated.

[4] Here we describe the fall of the Carancas meteorite, an H4-5 chondrite [H. C. Connolly, Meteoritical Bulletin no. 93, Meteoritics and Planetary Science, v.43, in preparation, 2008] on 15 September 2007 which produced a crater of ~ 14 m diameter. This event is particularly unusual

¹Department of Physics and Astronomy, University of Western Ontario, London, Ontario, Canada.

²EES-2, Atmospheric, Climate and Environmental Dynamics Group-Meteorological Modeling Team, Los Alamos National Laboratory, Los Alamos, New Mexico, USA.

³Department of Earth Sciences, University of Western Ontario, London, Ontario, Canada.

⁴Geological Survey of Canada, Pacific Division, Natural Resources Canada, Vancouver, British Columbia, Canada.

⁵Dpto Astronomia, Facultad Ciencias, Montevideo, Uruguay.

⁶Department of Geoscience, University of Calgary, Calgary, Alberta, Canada.

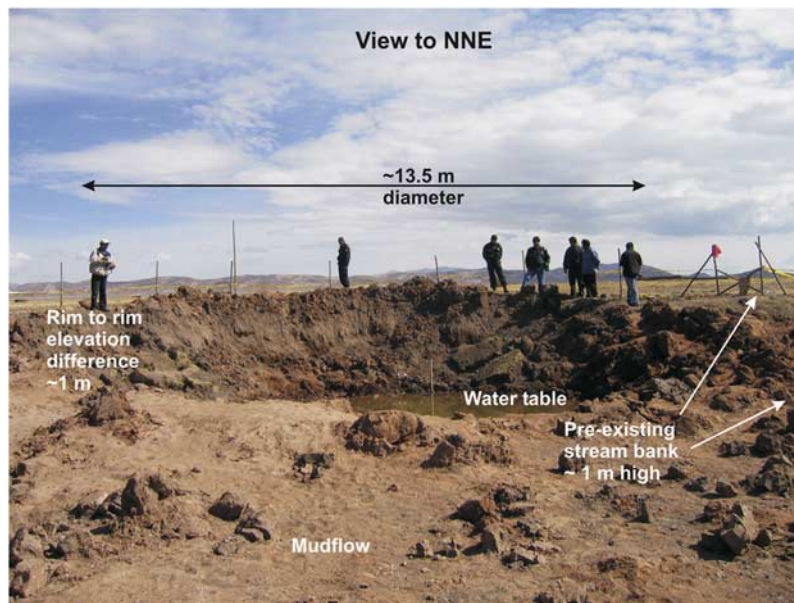


Figure 1. The crater 7 days after formation.

in that this large crater was produced by a chondritic meteorite. The present work concentrates on understanding and constraining the initial mass and velocity of the impactor and relating that to basic observations of the crater proper. While no optical recordings of the associated fireball are available, thanks to the global instrumentation provided by the International Monitoring System (IMS) of the Comprehensive Test Ban Treaty Organization, records of the infrasound waves from produced by the fireball passage have been recorded at stations IS08 and seismic station LPAZ and permit much of the analysis which follows.

2. Crater and Fireball Observations

[5] A bright fireball was observed by many eyewitnesses in Bolivia and Peru mid-day on 15 September 2007. The fireball was widely reported to have occurred near 1145 local time (1645 UT). Several eyewitnesses interviewed by G. Pereira (personal communication) described the fireball as being nearly as bright as the sun and loud detonations were recorded in the area. Significantly, eyewitnesses interviewed by Pereira at Guaqui, Bolivia reported the fireball as descending vertically, suggesting the true azimuth of the fireball path lies close to the line connecting Guaqui with the crater (azimuth of 71°). Residents of the border town of Desaguadero reported seeing the fireball/dustcloud to their South. Eyewitnesses located between Desaguadero and Azafranal at a ground location near 16.6°S , 69.0°W , who were facing South, observed the fireball heading from left to right, consistent with the observations from Guaqui. Finally, observers located near 17.0°S , 69.2°W some distance to the SSW of the crater reported the fireball to their North moving from right to left. These data suggest a basically East to West orientation to the entry flight path.

[6] Shortly after the fireball's appearance a large explosion was noted in the Carancas area of Peru by eyewitnesses, at least one of whom was only 300 m from the

subsequently formed crater. The crater is located at $16^\circ39'52''\text{S}$ and $69^\circ02'38''\text{W}$.

[7] The nearly circular 13.5 m crater spans part of the channel and bank of an ephemeral stream and the adjacent lake plain related to a Pleistocene stand of Lake Titicaca [Argollo and Mourguiart, 2000]. Total relief between the channel floor and the top of the bank is ~ 1 m. The lake plain is underlain by cohesive muddy lacustrine sediments. The difference in elevation of ~ 1 m between the high (north) and low (south) sides of the crater is largely an artifact of the former topography. The water table at the time of impact was less than about 50 cm below the bed of the ephemeral stream channel about ~ 1.5 m below the lake plain so that the impactor immediately came into contact with water-saturated unconsolidated argillaceous sediments. The maximum depth of the crater was not determined because it almost immediately filled with water and slumping sediment from the crater walls. Figures 1 and 2 show the crater as it appeared 7 days after the impact and Figure 3 shows the surface expression 46 days after the impact. Viewed from the north rim of the crater, ejecta consisting of angular fragments of lake sediment stretched predominantly for about 200 m from the SSE to the WNW of the crater. Though the analysis of the ejecta and the formation of the crater are a topic for a separate detailed study, a preliminary visual inspection of the distribution of the ejecta by one of us (GT) visiting the site 45 days after the impact, points to an asymmetry in the pattern. The farthest ejected material was found in the SW direction. Areas to the north and northeast of the crater were comparatively free of ejecta.

[8] Formation of the crater and eruption of the ejecta were closely followed by a mudflow from the crater into the ephemeral stream channel. This mudflow either buried or partly buried angular ejecta blocks within 10 to 15 m of the crater rim along the ephemeral river channel and apparently occurred immediately after impact when steam was rising from the crater. Muddy water, driven by the short-lived shallow heat source created beneath the crater by the impact

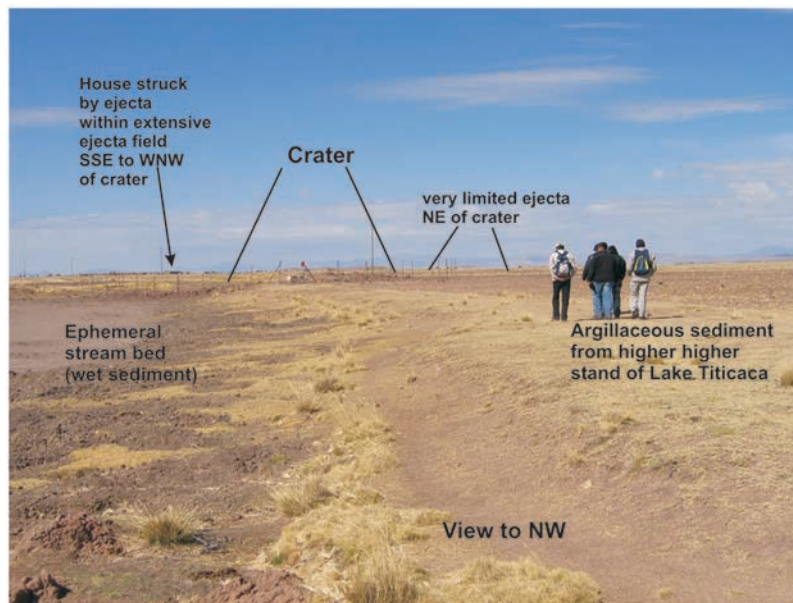


Figure 2. The geological context of the crater.

compression of the soil apparently rose above the lowest crater rim and poured out. This heating of fetid, anoxic mud to steaming is a possible source of the noxious fumes reported by many who arrived at the crater shortly after impact.

3. Infrasound Data

[9] Infrasonic records from the five closest microbarometer stations of the International Monitoring System (IMS) which had data for this date were examined for potential infrasound signals associated with the fireball/crater production. These included (distance from crater in brackets), IS08 (81 km) in Bolivia, IS41 (1620 km) in Paraguay, I09BR (2250 km) in Brazil, I14CL (2240 km) in Chile and I02AR (4220 km) in Argentina. Of these stations only IS08 and IS41 had signals clearly associated with the event. In what follows we describe and interpret the infrasound data from each station. Figure 4 shows the location of the infrasound and seismic stations in relation to the crater. The infrasound array analysis follows the standard techniques which are described in more detail elsewhere [Evers and Haak, 2001; Edwards et al., 2006].

3.1. IS08 Signal

[10] Fortunately, the fireball and crater occurred a very short distance from one of only 5 active infrasound arrays in South America. The first infrasonic wave train from the fireball at IS08 begins at 16:44:19 UT (for sensor #4) and is followed ~ 20 seconds later by a second distinct arrival (Figure 5). Table 1 summarizes the signal properties of each of the wave trains. The spectrum of each wave train shows infrasound energy up to the Nyquist cutoff of the instruments (9 Hz). This is consistent with a source very close to the station. These signals show a high cross correlation across the array with an unbounded Fisher Statistic [cf. Evers and Haak, 2001] above 20 while the average for the background is 1.4 for the half hour interval before and after

these events. Note that the crater is located some 81 km from IS08 at an apparent backazimuth of 231.6° .

[11] To analyze both wave trains in detail we manually chose a range of window sizes and band passes isolating each wave train in turn and performing an F_k analysis, which localizes the signal backazimuth and trace velocity assuming a planar wavefront across the microphone array. As a secondary check, we employed the Progressive Multi-Channel Correlation (PMCC) algorithm [Cansi, 1995] in an effort to verify these results. The basis of PMCC is a measure of the consistency of delay times (obtained using pairwise cross-correlation) for a given set of wave parameters—in our case backazimuth and trace velocity. If the consistency falls below a threshold, a detection is declared. PMCC results were obtained after filtering from 0.5 – 4 Hz and using 10 s time windows, with 75% overlap. Ten frequency



Figure 3. Crater as it appeared on 31 October 2007 (looking from NE to SW).

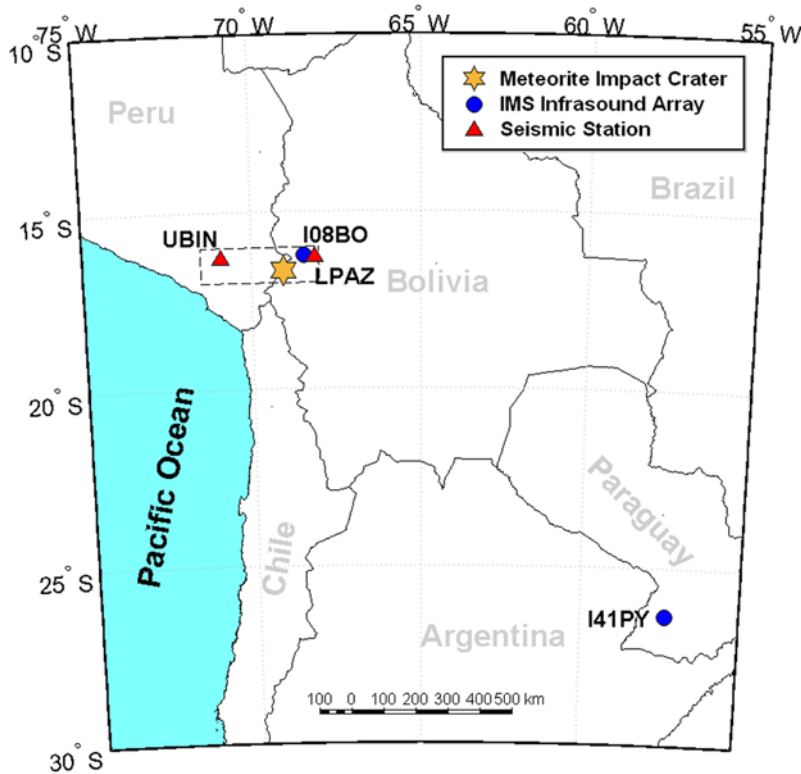


Figure 4. Large-scale map showing location of the crater in relation to seismic and infrasound stations which may have detected the airwave from the fireball/crater formation.

bands were used in the processing (covering the 0.5 - 4 Hz range where most energy is concentrated in the spectra of the signals), where the basic detection criteria is applied for each time window and frequency band. A nearest neighbor search method is then used to cluster elementary detections into “families”. The errors in each value (backazimuth and trace velocity) represent the standard deviation of values within each family.

[12] Both techniques show the backazimuth decreasing in time between wave train #1 to wave train #2. Our manual technique yielded a consistent backazimuth for train #1 over many window and band-pass combinations of $234.3^\circ \pm 3.4^\circ$

with a trace velocity of 0.352 km/s for the first infrasound arrival as compared to the PMCC analysis which resulted in a backazimuth of $227.4^\circ \pm 1.2^\circ$ and a trace of 0.346 km/s. Given the large formal errors in backazimuth, we consider that these two estimates are basically in agreement.

[13] The second wave train was analyzed in the same manner and a backazimuth value of $213.7^\circ \pm 2.3^\circ$ with a trace velocity of 0.336 km/s was most consistently found from manual examination. For comparison, the PMCC analysis of this second arrival found $215.4^\circ \pm 0.7^\circ$ for the backazimuth and 0.348 km/s for the trace velocity; these agree to within error. One uncertainty in the measurement of

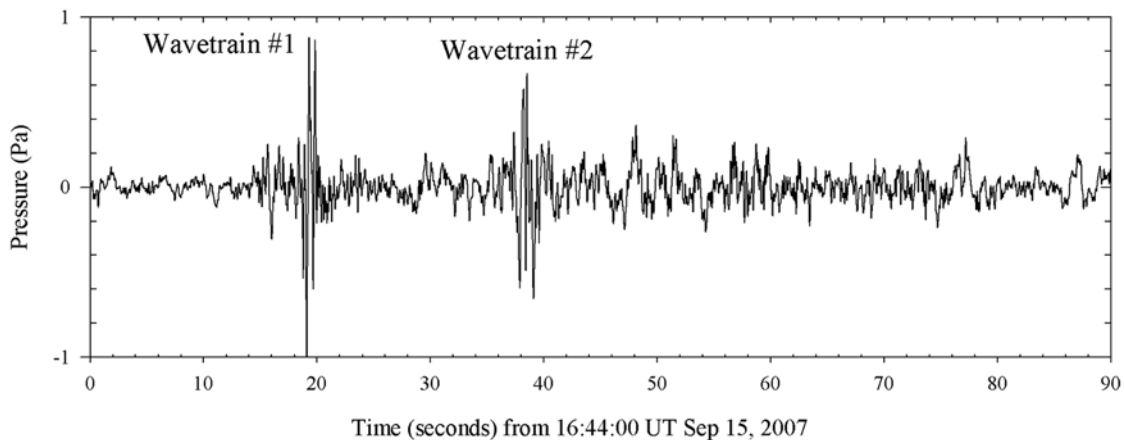


Figure 5. Airwave as detected at IS08. The signal shown is from element #4 and has been band passed from 0.3 to 8 Hz.

Table 1. Summary of Infrasound Signals Detected at IS08BO^a

Signal Property	Wave Train #1	Wave Train #2
Zero-Peak amplitude, Pa	0.76 ± 0.21	0.59 ± 0.14
Peak-Peak amplitude, Pa	1.91 ± 0.51	1.19 ± 0.25
Period at maximum amplitude, s	0.52 ± 0.03	0.62 ± 0.20
Arrival time (element #4) (UTC)	16:44:19	16:44:38

^aSignals have been band passed from 0.3 to 8 Hz. Errors represent the standard deviation across all four elements.

the second wave train is that some manual combinations of windowing and band passes suggest this could be a very steep return, with trace velocities as high as 0.75 km/s, while still maintaining similar backazimuths. Such a steep arrival angle for the infrasonic signal would imply a source location nearly overhead from IS08.

3.2. IS41 Signal

[14] Figure 6 shows the infrasound signal as detected at IS41. The association with the fireball/crater is more difficult in this instance because of the high background noise levels on the first two microphones; the infrasound signal is most obvious in the pressure data from array elements 3 and 4, beginning shortly after 1810 UT. The azimuth from the station to the crater is 309.1° . From manual windowing, the observed backazimuth is $308.7^\circ \pm 3.1^\circ$ while from PMCC analysis the value is $309.5^\circ \pm 0.2^\circ$. This agreement with the direction to the crater together with the delay time of ~ 5350 s corresponding to a mean signal speed of 0.303 km/s (which is consistent with a stratospheric infrasound arrivals; *Ceplecha et al.* [1998]) makes the signal association with the fireball/crater highly probable. A notable feature of the signal as seen from IS41 is its low amplitude (peak-to-peak amplitude < 0.05 Pa), almost two orders of magnitude lower than the detection at IS08 and comparable to the background noise level.

[15] Attempts to detect any correlated signal associated with the fireball using a range of possible average signals

velocities (from 0.20–0.40 km/s) over a wide range of passband combinations produced no detectable signals at I09BR, I14CL and I02AR.

4. Seismic Data

[16] At least one seismic station (LPAZ) detected air-coupled Rayleigh waves from the fireball and another (UBINS) may also have detected the infrasonic signal. In both instances our best interpretation based on timing suggests these are from the ballistic shock created by the fireball as opposed to the infrasound signal generated at the time of crater formation by that explosion or by surface waves from the impact itself.

[17] The closest seismic station was LPAZ, located 106 km to the ENE of the crater. Figure 7 shows the vertical component of ground velocity for LPAZ from 1615–1715 UT measured by the short-period sensor. Examination of the hour of data centered around 1645 shows numerous short-duration events like that at 1637. We associate these with microseismic activity which is continuously visible in the LPAZ records. The unusual waveform beginning near 1644 UT (with a beginning at 16:44:42 UT and peaking at 16:45:45 UT which we take as the most probable infrasound signal arrival time for our initial analysis) is phenomenologically similar to air-coupled Rayleigh waves detected seismically from other fireballs [*Edwards et al.*, 2006]. We have applied a minimization constraint for the energy of the reconstructed transverse component at LPAZ to determine probable arrival direction (which is among the most robust techniques for high-noise seismic data). In this approach we apply a series of rotations to the horizontal components of the seismic signal and measure the transverse energy; the angle producing the minimum in the transverse energy is taken to be the most probable arrival azimuth. The radial direction in this case will correspond to the propagation direction for either directly coupled air

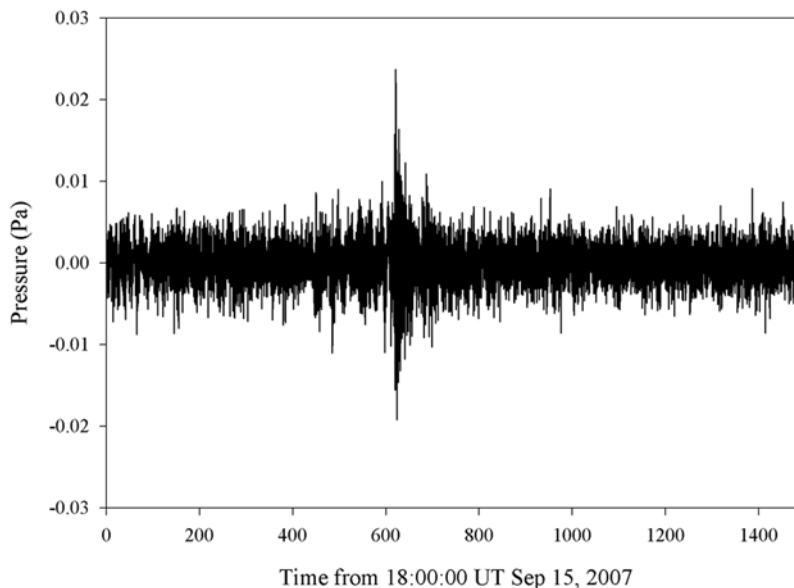


Figure 6. Fireball airwave as detected at IS41 shown on element #3. The signal has been band passed from 0.5 to 4 Hz. Time is in units of seconds.

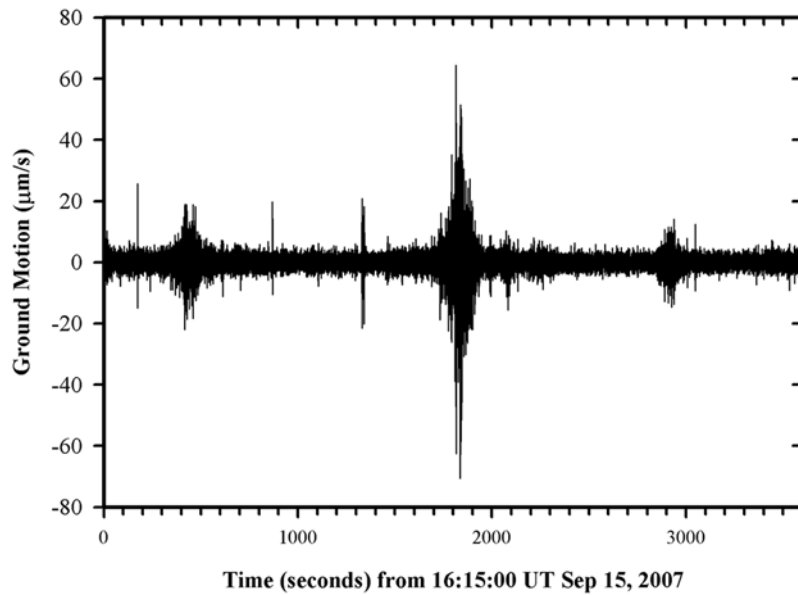


Figure 7. Seismic signal at LPAZ. The data shown are for the vertical component of the short-period seismometer and are not band passed.

arrivals or air-coupled Rayleigh waves. We find a best fit arrival direction of 140° with a 180° potential azimuth ambiguity (i.e., either 140° or 320° is possible) in the 8 – 17 Hz passband. The error using this technique is difficult to quantify. In particular, different choices of band-pass filter parameters produce quite different azimuths for our data given the extremely low signal to noise ratio. We can neither definitively associate or rule out connection with the fireball infrasonic signal on the basis of this azimuth measurement alone and note that scattering from the significant terrain in the area may complicate the apparent arrival direction.

[18] The seismic data from UBINS is more problematic. Four separate 3 component seismic stations detected a potential signal from this location, on the side of a volcano near Moquegua. Figure 8 shows the band passed vertical component of the signal, observed by one of the four stations, the other stations show similar signals. As with LPAZ, there is a dispersed signal peaking near 16:55:07 UT which appears on all four instruments and which is similar in character to other fireball infrasonic - seismic coupling events and to the LPAZ waveform. However, these data are quite noisy in the horizontal components and taking all four stations as an array and performing PMCC analysis does not

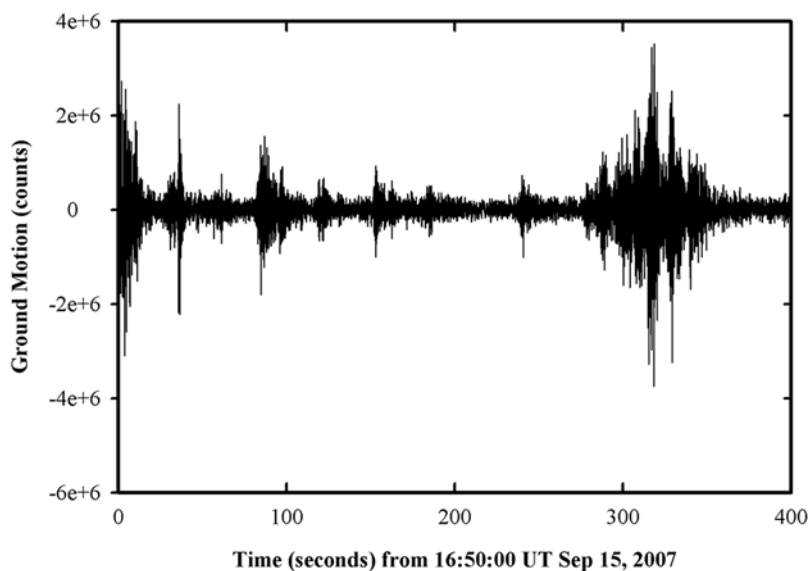


Figure 8. Seismic data from UBINS. Shown below are the raw (unfiltered) data from the vertical component of UBIN4. The other three nearly colocated seismic stations look similar. The prospective airwave signal peaks near $t = 300$ s in this plot.

produce any signals with backazimuths toward the crater. The horizontal components are used to estimate a common backazimuth for a signal linked to the fireball. The signals are relatively incoherent between the different stations, reflecting the very volcanically active region and associated high seismic noise. Thus we cannot confirm that this represents an infrasound signal associated with the fireball.

5. Trajectory and Orbit Constraints

[19] From the preceding measurements/observations some immediate constraints are available for the atmospheric trajectory for the fireball. The strongest is the eyewitness observations in Guaqui which suggest a ground azimuth for the path near 71° . From previous experience interviewing fireball eyewitnesses [Hildebrand *et al.*, 2006], it is likely that this observation places the ground azimuth within about 10 degrees of 71° . From the IS08 infrasound data, the first arrival wave train points back almost exactly to the crater, with the PMCC results suggesting a pointing slightly east of the crater. One interpretation is that this represents infrasound signals from the last portion of the fireball trajectory shortly before impact. Another, perhaps simpler interpretation, is that this is the arrival of the infrasound signal created by the surface explosion which created the crater. Note that this signal travels with ground-level acoustic velocities across the array. On the basis of simultaneous inversion of local earthquake arrival-time data for velocity and hypocentral parameters, shallow (<5 km) crustal S-wave velocities (V_s) in the central Andes near LPAZ are $2.85 \text{ km/s} \pm 10\%$ [Dorbath and Granet, 1996]. Since Rayleigh surface waves are thus expected to propagate at group wave speeds of more than $\sim 2.36 \text{ km/s}$ (i.e., 92% of V_s), we do not believe any surface waves from the crater formation were detected at IS08, noting that the MB2000 infrasound sensors which are used at IS08 are known to act also as good seismometers.

[20] The second wave train shows a smaller backazimuth and arrives slightly later—this behavior is typical of fireball infrasound signals from earlier/higher in the trajectory. This suggests that the fireball was moving generally from East-West and to the South of IS08. Since the azimuth connecting IS08 to the crater is 52° , this further constrains the fireball azimuth to be larger than 52° . Our best fit trace velocity for this second wave train ($\sim 0.34 \text{ km/s}$) corresponds to a near horizontal arrival angle. However, given the potential ambiguity in the solution (see section 3.1), and the local effects of the planetary boundary layer we choose not to use this as a firm constraint.

[21] To construct a most probable trajectory we make use of the data from IS08 and LPAZ as the most reliable. The crater is taken to be the terminal ground point projection (i.e., the location where the straight line trajectory intersects the ground). We proceed on the assumption that the fireball likely did not experience significant fragmentation episodes, the strongest evidence for this being the survival of a substantial mass to the ground to form the crater. Under such an assumption, we expect the infrasound signal at each station to represent a ballistic arrival; that is an infrasonic wave propagating perpendicular to the trajectory in reaching the station (cf. *ReVelle* [1976] for details). Theoretical considerations and observations have shown that ballistic

arrivals may be produced for deviations up to $\sim 20^\circ$ from this limit [Brown *et al.*, 2007; Edwards *et al.*, 2007]. In addition to this constraint, we have the arrivals timing as a second constraint. Here we use a model atmosphere as generated from the UK Meteorological Office (UKMO) assimilated data set [Swinbank and O'Neill, 1994] for winds below 65 km height supplemented with NASA and Naval Research Labs MSIS-E00 and Horizontal Wind Models (HWM) [Hedin, 1991; Hedin *et al.*, 1996] for temperature and winds over 65 km altitude at the time and location of the crater formation. Point source ray tracing was performed using the InfraMap [Gibson and Norris, 2000] utility coupled to this model atmosphere. Raytracing from the crater to IS08 suggests that any infrasound signals which might arrive would have a travel time of 242 sec from crater production to arrival of the 1st infrasound signal at IS08, presuming the 1st wave train at IS08 is from crater production.

[22] Applying the ballistic constraint for IS08 coupled with the apparent backazimuth of the second wave train (215.4°) we find that the trajectory solutions meeting this criteria have either low-entry angles ($15\text{--}40^\circ$) and pass just south of IS08 (up to a radiant azimuth of 58°) or have slightly steeper entry angles ($41\text{--}48^\circ$) with azimuths from $82\text{--}110^\circ$. These combinations of radiant azimuth/elevation do not produce correct timings at IS08 and LPAZ and so are discarded from further consideration. However, for trajectory azimuths beyond 58° and entry angles above 45° strict ballistic solution to IS08 no longer exist. The closest paths to ballistic for IS08 occur at a fireball azimuth of 66° for all entry angles above this value. Unfortunately, none of these strictly ballistic solutions can simultaneously match the observed timing between IS08 and LPAZ—for most cases the solutions would suggest that the infrasound signals should be detected at LPAZ first (which is clearly not observed). Furthermore, the timings do not match the relative temporal spacing between the 1st wave train arrival (presumed to be from the crater) and the 2nd wave train at IS08. Recognizing that these timings are likely a more stringent constraint than the ballistic geometry (which can show deviations of up to tens of degrees) we relax the ballistic constraint for IS08 and search for the closest to ballistic for IS08 solution (which is still ballistic for LPAZ) which matches the arrivals at IS08, LPAZ and still retains the relative timing between the 1st and 2nd infrasonic arrivals at IS08.

[23] Employing this approach and searching across a grid spaced at 1 degree increments in azimuth and elevation we find a best fit trajectory solution having an azimuth of 82° , and a reasonably steep entry angle of 63° . We note that the deviation from a ballistic arrival is 25° for this solution relative to IS08 placing it near the upper end of previously observed deviations (cf. *Edwards et al.* [2007] who refer to such arrivals as quasi-ballistic). This solution also establishes the time of formation of the crater as 16h 40m 17s UT. Figure 9 shows this trajectory plotted on a regional scale map of the fall area, together with the IS08 backazimuth measurements. We emphasize that this cannot be considered a unique solution, but rather representative on the basis of the assumptions just outlined.

[24] With this proposed trajectory solution we may also examine potential pre-atmospheric orbits for additional constraints on the entry velocity. In particular, *Wetherill and ReVelle* [1982] show that meteorite-producing fireballs

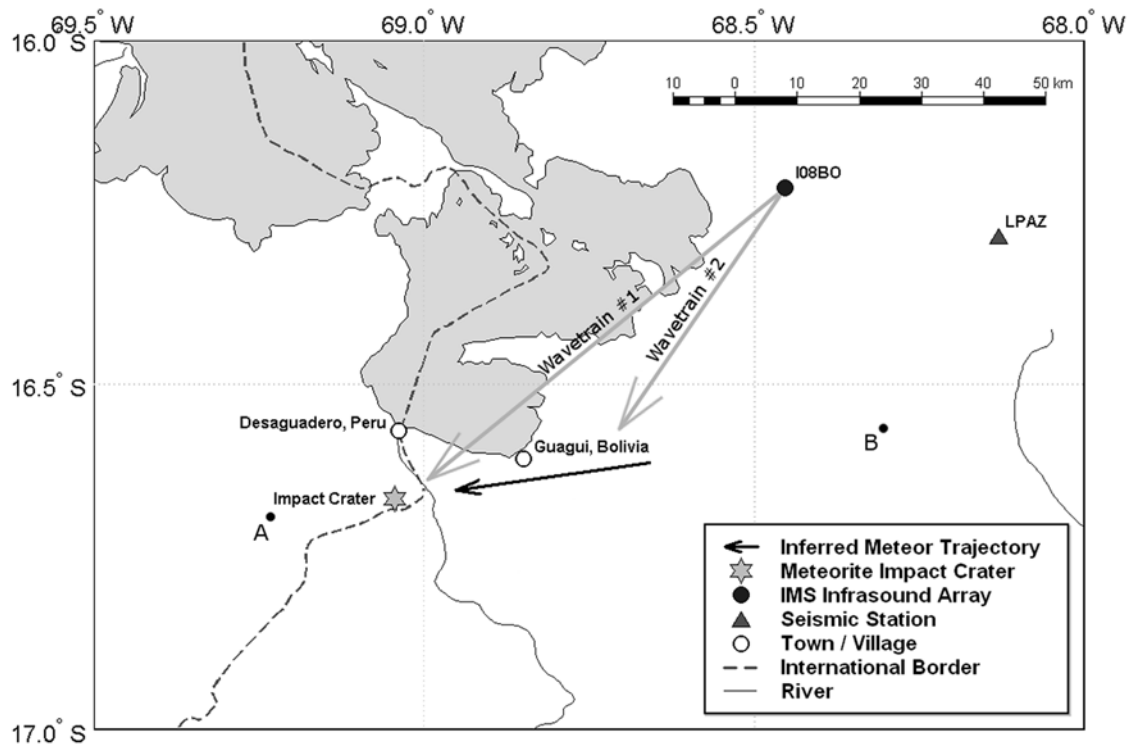


Figure 9. Regional map showing the preferred fireball trajectory. The trajectory is shown beginning at a height of 80 km for our preferred trajectory orientation. Both infrasonic wave train backazimuths from IS08 are also shown for comparison.

are rarely in trans-Jovian orbits. Another measure of this constraint is to require that the Tisserand parameter with respect to Jupiter be larger than 3 [Levison, 1996]. Table 2 shows the orbit solutions for our best fit radiant azimuth and altitude. The orbit becomes trans-Jovian for initial velocities above 16.9 km/s. This suggests that the initial meteoroid velocity at the top of the atmosphere must have been between 11.7–16.9 km/s.

[25] As an independent check on this solution, we may apply the weak-shock overpressure/period approach [ReVelle, 1976; Edwards et al., 2007] to this trajectory relative to IS08 for plausible meteoroid velocities and masses (see section 6) to check for consistency in the observed overpressure and period. Figure 10 shows the expected overpressure as a function of height (terminating at the altitude of IS08) for the full range of velocity/masses predicted in section 6. The predicted period from the weak-shock model is within error of that observed at IS08 for the low-mass/low-velocity case; the overpressure is more than a factor of two higher in the model than observed. This difference in overpressure is well within typical variations previously noted for fireballs with independent optical–infrasound records [Edwards et al., 2007]. The higher-velocity/mass curves show even larger differences in overpressure and much larger periods. The overpressure is particularly sensitive to height–heights below 55 km produce overpressure estimates more than an order of magnitude higher than observed and periods much longer than is observed. This suggests that the overpressure and periods measured at IS08 favor the lower velocity/mass combinations to be described in the next section, though the fits are less sensitive to mass

than velocity. This measurement also rules out shallow entry angles.

6. Meteoroid Entry Modeling

[26] Having established a preferred trajectory and narrowing entry velocity limits in the previous section we attempt to model the entry of the meteoroid. For this procedure we use the diameter of the crater as a constraint. We note that given the crater size (13.5 m) and the expected diameter range of the impactor (~ 1 m), the crater may be near the transition from material strength scaled cratering to gravity scaled cratering [Holsapple, 1993] depending on the yield strength of the local soil, though ostensibly it is still in the strength scaled regime. Scaling relations in this transition range are not well established, so for a fixed impact velocity and impact angle we can expect final masses to vary by factors of several depending on the approach used.

Table 2. Potential Orbital Solutions for the Best Fit Trajectory Having a Radiant at Azimuth = 82° and Entry Angle of 63° (Apparent Radiant $\alpha = 203.1^\circ$, $\delta = -11.2^\circ$)^a

V_∞ (km/s)	a (A.U.)	q (A.U.)	e	ω (deg)	i (deg)	T
12	1.22	0.9889	0.19	153.6	0.65	5.2
13	1.43	0.9698	0.32	148.5	0.57	4.6
14	1.64	0.9551	0.42	146.1	0.44	4.2
15	1.92	0.9428	0.51	144.5	0.31	3.8
16	2.29	0.9319	0.59	149.4	0.19	3.3
17	2.82	0.9222	0.67	142.5	0.08	2.9
18	3.69	0.9134	0.75	322.0	0.02	2.5

^aAll angular elements are J2000.0. T is the nondimensional Tisserand parameter with respect to Jupiter. The orbit for all velocities is typical of that of an Apollo-type asteroid.

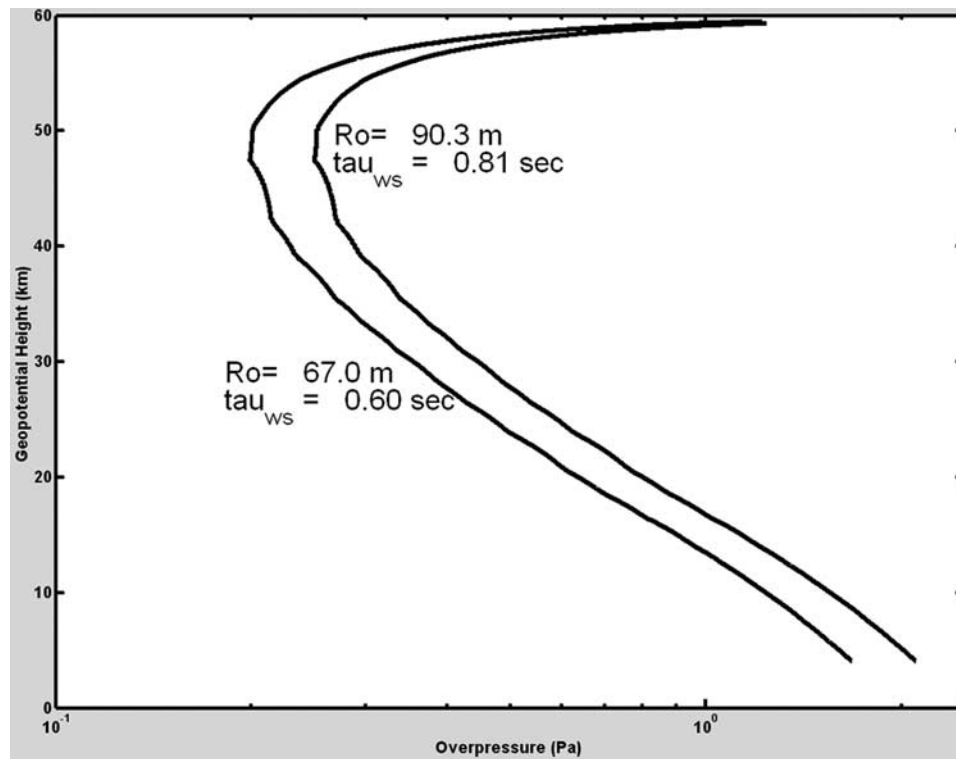


Figure 10. Predicted overpressure as a function of height based on the extreme range of blast wave radii (R_o) for our modeling solutions using a weak-shock model. The weak-shock periods at the ground are shown for each of the extreme values of blast radius. The lower value for the blast radius (67.0 m) corresponds to modeling solutions, with masses of 6800 kg and velocity of 12.6 km/s, while the upper limit corresponds to values of 10,000 kg and $v = 14.9$ km/s all at 60 km height.

[27] Here we employ the crater scaling relation developed by *Gault* [1974] given by:

$$D = 2.5 \times 10^{-2} \rho_m^{\frac{1}{6}} \rho_t^{\frac{1}{6}} W^{0.29} (\sin \Theta)^{\frac{1}{3}} \quad (1)$$

where D is the crater diameter in meters, ρ_m is the mass density of the impactor (in units of kg^{-3}), ρ_t is the mass density of the target (in units of kg^{-3}), W is the kinetic energy of the impactor (in J) and θ is the impact angle from the horizontal. This relation applies to craters formed in loose soil, which is reasonably appropriate in our case. Other scaling relations [cf. *Holsapple*, 1993] were compared to this result and found to produce values within $\sim 20\%$ in terms of crater diameter for modestly hypersonic impact velocities (1–6 km/s). Given large uncertainties in material properties, crater scaling relations in general and the large role water saturation can play in such cratering [*Melosh*, 1989] we feel this relation is as representative and appropriate as anything else available in the cratering literature.

[28] Taking this crater size–impactor energy/mass/size relation, we have a range of end masses/velocities consistent with the crater size. We next model the ablation behavior of the meteoroid in the atmosphere, making use of the orbital constraint determined in the previous section to limit our initial velocities between 11.7–17 km/s.

[29] The first model we employ is that of *ReVelle* [2005]. This model includes luminosity output based on an ener-

getics end height approach (see also *ReVelle* [2001a, 2001b] for more details of parameters used in the model). For this application we use a bottom up approach by searching for an inverse solution, using combinations of initial masses, entry angles and entry velocities which produce the crater of the correct size (with a crater size tolerance of ± 2 m and an end height tolerance of 0.5 km) observed at the ground. The variables chosen for ablation parameters, porosity and density (3300 kg^{-3}) of the impactor were those appropriate to type I fireballs, which are believed to be related to ordinary chondrites [*Cepilecha et al.*, 1998]. We explicitly do not allow any significant fragmentation in this approach—incorporation of fragmentation generally will move our estimated initial masses to higher values if everything else remains the same. Figure 11 shows the family of solutions from this modeling in terms of initial mass and entry velocity as a function of entry angle. The modeling does not find any suitable combination of initial mass and velocity for entry angles below 48 degrees. Moreover, the model independently predicts no solutions for velocities above 15.5 km/s at any entry angle, in agreement with the constraints from orbital considerations. For our favored trajectory/entry angle the model also predicts minimum masses reaching the ground of 1000–1600 kg with predicted impact velocities at the ground of 3–4 km/s. Initial masses range from 3100–8500 kg with equivalent initial kinetic energies of 0.06–0.23 kilotons (kT) of TNT equivalent (1 kT TNT = 4.185×10^{12} J). This model also suggests that the peak absolute magnitude of the event was between -17 and

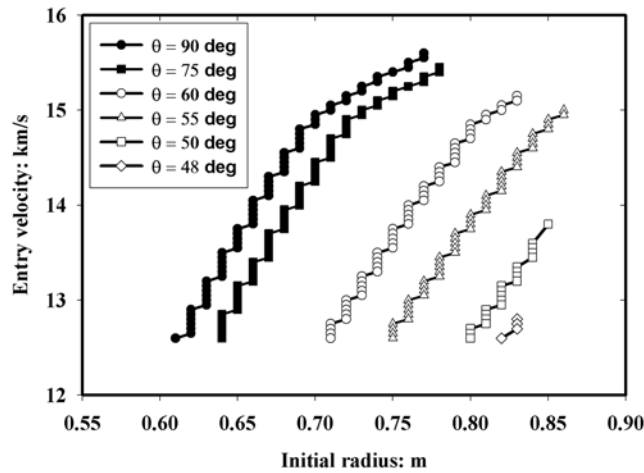


Figure 11. Inverse entry model using a nonisothermal hydrostatic summer model atmosphere and no fragmentation. Model results show required initial radius of meteoroid (assumed density of 3300 kg^{-3}) as a function of allowable entry velocities and entry angles (θ —measured from the horizontal) to produce a crater of the final observed diameter.

–20, consistent with eyewitness observations reporting brightnesses approaching that of the sun.

[30] As a simple check on this detailed result, we also apply the gross fragmentation model of *Ceplecha et al.* [1993]. Here again we assume explicitly that no significant fragmentation occurs during flight so that the motion truly is that of a single-body. We make use of the recent work of *Ceplecha and ReVelle* [2005] who show, in particular, that the intrinsic ablation coefficient (i.e., without implicitly accounting for fragmentation) for meteorite producing fireballs is generally in the range $0.004\text{--}0.008 \text{ s}^2\text{km}^{-2}$. Using these bounding ablation coefficients (as constants) and the range of $12\text{--}17 \text{ km/s}$ for entry velocity constrained from the orbital considerations (with all other parameters corresponding to type I fireballs as in the previous model and using our favored trajectory solution) we again imposed the constraint that our final kinetic energy must produce a crater of the observed size (13.5 m in diameter) using equation (1). Figure 12 shows the initial and final masses under these simplified modeling assumptions. Our range of initial masses is nearly identical to that found from the earlier, more detailed model; in the present model initial masses range from $5700\text{--}9100 \text{ kg}$ and equivalent initial kinetic energies vary from $0.1\text{--}0.32 \text{ kT TNT}$. Figure 12c shows the velocity as a function of time for the extreme initial velocities in the model.

[31] The main difference between the models is in the final end height conditions. The final masses in this model are a factor of $2\text{--}3$ larger and the final impact velocities $\sim 1/2$ that of the *ReVelle* model. This disparity is due to the different manner in which velocity depends on the ablation coefficient in the two models (cf. *ReVelle* [2005] for details). In the discussion which follows we will use the results from the model of *ReVelle* [2005]. An interesting point brought out by both models is that the high altitude of the impact location (3800 m above sea level) is a major contributor to the size of the crater. Had the object impacted at sea level,

the crater would have been less than half its observed size and the impact velocity would have been only mildly supersonic.

7. Discussion

[32] From the foregoing analysis it is clear that the problem of fireball trajectory reconstruction is not highly constrained; we have made a number of assumptions in arriving at our favored trajectory model (radiant azimuth of 82° and entry angle of 63°). If the infrasonic arrival at LPAZ, for example, is taken to be the very start of the signal waveform (instead of its amplitude peak) the trajectory solution moves to a lower azimuth (near 75°) and steeper entry angle ($\sim 70^\circ$). The uncertainties in the launch angle of a ballistic wave to either IS08 or LPAZ produce another set of uncertainties which lead to comparable possible variations in the radiant location. We can state, however, that the preponderance of the eyewitness observations and infrasonic data from IS08 in particular favor a fireball trajectory coming from the E or ENE with the ejecta pattern at the crater generally supporting this notion.

[33] The interpretation of the first infrasonic arrival at IS08 leads to two potential scenarios. The simplest is that this represents the infrasound signal produced from the explosion of the crater. The main difficulty with this interpretation is that for the UKMO model atmosphere used for this date/time/location, acoustic rays from the crater have no direct path to IS08 from the crater. Our modeling with *InfraMap* does not account for the significant topography between the crater and IS08. Indeed, the terrain first increases in altitude away from the crater in the direction of IS08 before decreasing again. This topographic barrier makes it even more difficult for direct ray arrivals. It is possible that acoustic reflections from mountains and the rugged terrain produce arrivals at IS08 which are not direct and/or that the low-level winds differ from what is in the atmospheric model; in both cases these could lead to production of the first infrasonic arrival at IS08 from the crater. If we accept that this infrasound signal is from the crater formation (keeping in mind the outstanding issues with this direct interpretation), we may estimate its source formation energy by appealing to work done in calibration of energy of surface explosions using infrasound. From the first wave train arrival at IS08, we may use the relation developed by *Davidson and Whitaker* [1992] to include the effects of winds on the expected change in overpressure measured infrasonically. Their empirical relation connecting overpressure, source yield, range and wind velocity measured for high explosive surface changes takes the form:

$$\log E_S = 1.47 \log P_c + 2 \log R - 4.96 \quad (2)$$

where the ground range, R , is in kilometers and source energy, E_S , in kilotons of TNT equivalent explosive energy. Here P_c is the wind corrected amplitude in Pascals of the form:

$$P_c = 10^{kv_h} A \quad (3)$$

where A is the measured pressure amplitude, v_h is the horizontal component of the wind vector directed toward the receiver in meters/second and k is an empirical constant in seconds per meter. Using the model wind values and applying this relation to our observations we find an equivalent predicted yield of ~ 5 tons TNT. We remark that using various other yield-pressure-range scaling relations without expli-

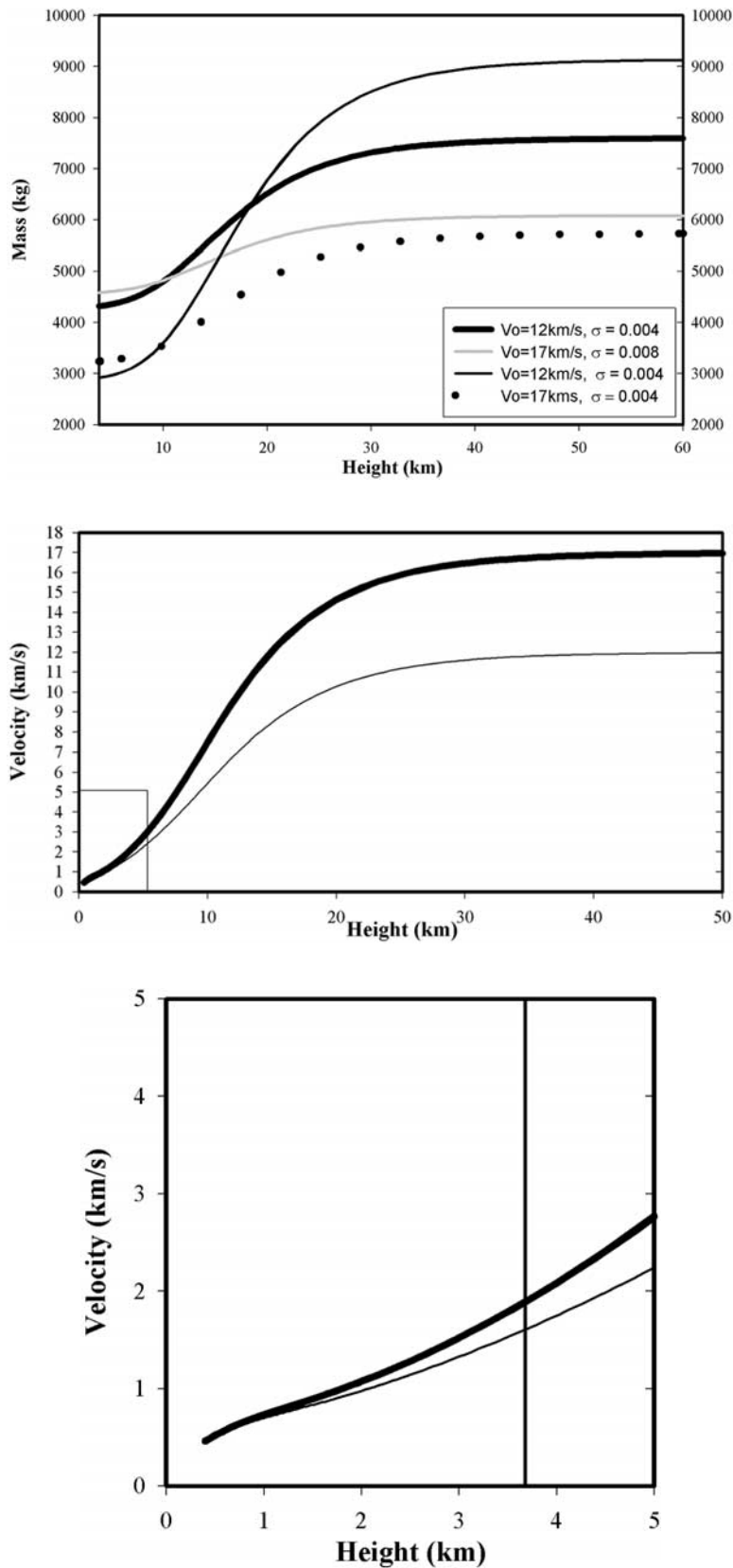


Figure 12. (top) Mass as a function of height for extreme values of the ablation coefficient and entry velocity. (middle) Velocity as a function of height (thick line = 17 km/s initial velocity, thin line = 12 km/s initial velocity). (bottom) Enlarged portion of the middle plot showing the modelled velocity difference between the actual impact site (vertical black line at 3.8 km altitude) and what the impact velocity would have been had the site been at lower elevations.

citly accounting for the effects of winds produces yields 1–2 orders of magnitude lower.

[34] The other interpretation is that this represents the ballistic wave from near the end of the fireball path, perhaps because of some low-altitude fragmentation. Using the PMCC measured backazimuth for the first infrasonic arrival at IS08 (227°) and intersecting this with our favored trajectory (azimuth 82° and entry angle 63°) produces a putative point at altitude 20 km some 11 km from the ground location of the crater. Ray tracing does produce ray paths to IS08 from this location. Using the results from the previous modeling section and taking the solution producing the smallest blast radius (56 m) at this height we find the predicted weak-shock overpressure at IS08 to be 22 Pa—more than an order of magnitude higher than is observed. Unless our model velocity or mass is much too high or this is a signal from a fragmentation event we rule this out as a plausible interpretation.

[35] Using the signal from IS41 we may apply the long-range empirical bolide energy estimation relations developed by *Edwards et al.* [2006] to derive an independent source energy estimate. As with the ambiguity in the first wave train observed at IS08, it is not entirely clear whether the infrasound signal arriving at IS41 relates to the crater formation or the latter stages of the fireball. In either instance, it should roughly correspond to the cratering energy presuming the signal does not come from early in fireball flight.

[36] Given the extreme variation in noisiness across all four channels at IS41 we choose to use the channel with the highest signal to noise (#3) and recognize that this represents an upper limit to the energy estimate. Using the crater–IS41 range and great circle component of the wind from our atmospheric model together with the observed signal amplitude (0.04 Pa peak-to-peak) we derive a source energy estimate of 3 tons TNT equivalent.

[37] The UBINS signal is difficult to reproduce with ray-tracing; the returns are counterwind and no direct acoustic paths from the crater to UBINS could be found. For our proposed trajectory the geometry is such that no ballistic returns should reach UBINS. We conclude that the tentatively identified signal on UBINS is probably not related to the fireball.

[38] Ground surface waves from the crater impact should have been produced, but the range at which these would be detectable is unclear. We can take our crater origin source time (16 h 40 m 17 s) and use a P-wave velocity of 5 km/s to estimate the arrival time for any direct ground wave at LPAZ. This produces an estimated time at LPAZ of 16 h 40 m 38 s. There is a small signal at 16 h 40 m 36 s, but LPAZ is replete with similar signals separated by only a few tens of seconds over the interval 16 h 30 m–16 h 45 m so this identification, while suggestive, is not confirmable with our data alone. Seismic stations closer to the crater might be able to detect any body or surface waves, but we find no evidence in these data for such waves.

8. Conclusions

[39] From our reconstruction of the probable trajectory of the fireball producing the crater near Carancas, Peru we find a most favored radiant for the fireball to be at an azimuth of 82° and entry angle of 63°. From this trajectory, potential

orbits which are not trans-Jovian constrain the entry velocity to be below 17 km/s. Entry modeling of this event suggests initial masses of 3–9 tons and initial energies of 0.06–0.32 kT TNT equivalent. The final impact velocity is estimated to be in the range of 1.5–4 km/s and the final mass upon impact is of order a metric ton. Infrasonic pressure amplitude measurements using several different approaches correspond to source energies of 2–3 tons TNT equivalent for crater formation. All of these estimates are comparable to the 1.5 tons TNT equivalent impact kinetic energy predicted from equation (1). From this modeling alone we predict few or no impact shock effects proximal to the crater and suggest that much of the mass of the original impactor has been spalled out of the crater and/or the mass remaining in the crater is in the form of disaggregated small fragments.

[40] The most unusual aspect of this crater-forming impact is the nature of the impactor. In general, chondritic meteorites break up during atmospheric flight and do not reach the surface as large objects with a significant fraction of their pre-atmospheric speed. The peak dynamic pressure experienced by the Carancas impactor from our modeling is <30 MPa, while the most probable is just over 15 MPa based on our most probable entry velocity near 12 km/s. This is comparable to the typical “strongest” fireball material which experiences main fragmentation above ~12 MPa [*Ceplecha et al.*, 1998], though we note there is a considerable spread in the strengths of chondritic-like fireballs and no clear correlation between strength and mass. The tensile strength of ordinary chondrites averages ~20 MPa, but the spread from measured meteorites is almost an order of magnitude [*Petrovic*, 2001]. This emphasizes the great range in strength amongst individual meteorites, a trend we also expect to be reflected in pre-atmospheric meteoroids. Thus a strong, coherent stony object with few shock cracks could likely withstand the pressures most of our models predict for Carancas (based on lab measurements of meteorite strengths) and experience mild or no fragmentation as opposed to the catastrophic fragmentation typical for chondrites. It is notable that the largest single-mass chondritic meteorite, Jilin, at 1170 kg is comparable to the mass range we estimate for the Carancas meteorite and that the original estimate for this impacting mass just before contact with the soil was 2 tons. In the spectrum of pre-atmospheric strengths, it seems most probable that the Carancas chondrite was simply at the statistical high-end of the strength distribution, thus accounting for the large single mass to impact near Carancas. Finally, we observe that the unusually friable nature of the recovered meteorite fragments [*Nunez del Prado et al.*, 2008] would be explained in our hypothesis as being due to significant shock disaggregation at impact.

[41] **Note added in proof.** As this article was going to press, another analysis of the infrasound and seismic data associated with the Carancas fall has also appeared (A. Le Pichon et al., Evidence of a meteoritic origin of the September 15th, 2007 Carancas crater, *Meteoritics and Planetary Science*, 2008). Using additional data from several seismic stations closer to the crater than were available for our analysis, this study finds similar source energies to

the values we describe and a trajectory solution that is within error of our best fit solution.

[42] **Acknowledgments.** P.G.B. thanks the Natural Sciences and Engineering Research Council of Canada and the Canada Research Chairs program for support. The authors thank Dr. Hernando Tavera from the Instituto Geofísico del Perú for making available the seismic data from the UBINS site and G. Pereira from Observatorio Astronómico de Patacamaya for providing information from several witnesses. We thank the British Atmospheric Data Centre for access to the UKMO upper air weather data. The authors gratefully acknowledge helpful discussions with J. Melosh and A.R. Hildebrand.

References

- Argollo, J., and P. Mourguiart (2000), Late Quaternary climate history of the Bolivian Altiplano, *Quat. Int.*, 72, 37–51.
- Brown, P. G., A. R. Hildebrand, D. W. E. Green, D. Page, C. Jacobs, D. ReVelle, E. Tagliaferri, J. Wacker, and B. Wetmiller (1996), The fall of the St-Robert meteorite, *Meteorit. Planet. Sci.*, 31, 502–517.
- Brown, P. G., W. N. Edwards, D. O. ReVelle, and P. Spurny (2007), Acoustic analysis of shock production by very high-altitude meteors. I: Infrasonic observations, dynamics and luminosity, *J. Atmos. Sol.-Terr. Phys.*, 69, 600–620.
- Cansi, Y. (1995), An automatic seismic event processing for detection and location: The P.M.C.C. method, *Geophys. Res. Lett.*, 22(9), 1021–1024.
- Ceplecha, Z., and D. O. ReVelle (2005), Fragmentation model of meteoroid motion, mass loss, and radiation in the atmosphere, *Meteorit. Planet. Sci.*, 40, 35.
- Ceplecha, Z., P. Spurny, J. Borovička, and J. Kečliková (1993), Atmospheric fragmentation of meteoroids, *Astron. Astrophys.*, 279, 615–626.
- Ceplecha, Z., J. Borovička, W. G. Elford, D. O. ReVelle, R. L. Hawkes, V. Porubčan, and M. Simek (1998), Meteor phenomena and bodies, *Space Sci. Rev.*, 84, 327–471.
- Davidson, M., and R. W. Whitaker (1992), Miser's gold, *Los Alamos National Laboratory Report LA-12074-MS*, pp. 1–28.
- Dorbath, C., and M. Granet (1996), Local earthquake tomography of the Altiplano and the Eastern Cordillera of northern Bolivia, *Tectonophysics*, 259, 117–136.
- Edwards, W. N., P. G. Brown, and D. O. ReVelle (2006), Estimates of meteoroid kinetic energies from observations of infrasonic airwaves, *J. Atmos. Sol.-Terr. Phys.*, 68, 1136–1160.
- Edwards, W. N., P. G. Brown, R. J. Weryk, and D. O. ReVelle (2007), Infrasonic observations of meteoroids: Preliminary results from a coordinated optical-radar-infrasound observing campaign, *Earth Moon Planets*, doi:10.1007/s11038-007-9154-6.
- Evers, L. G., and H. W. Haak (2001), Listening to sounds from an exploding meteor and oceanic waves, *Geophys. Res. Lett.*, 28(1), 41–44.
- French, B. M. (1989), Traces of catastrophe: A handbook of shock-metamorphic effects in terrestrial meteorite impact structures, *Tech. Report, LPI Contribution No. 954*, 120 pp., Lunar and Planetary Institute, Houston, Tex.
- Gault, D. E. (1974), Impact cratering, in *A Primer in Lunar Geology*, edited by R. Greeley and P. Schultz, pp. 137–175.
- Gibson, R., and D. Norris (2000), The infrasound analysis tool kit InfrMap: Capabilities, enhancements and applications, in 22nd Seismic Research Symposium, Defense Threat Reduction Agency, New Orleans, La., 6 Jul.
- Hedin, A. E. (1991), Extension of the MSIS thermospheric model into the middle and lower atmosphere, *J. Geophys. Res.*, 96, 1159–1172.
- Hedin, A. E., et al. (1996), Empirical wind model for the upper, middle and lower atmosphere, *J. Atmos. Terr. Phys.*, 58, 1421–1447.
- Hildebrand, A. R., P. J. A. McCausland, P. Brown, F. J. Longstaffe, S. Russell, E. Tagliaferri, J. F. Wacker, and M. J. Mazur (2006), The fall and recovery of the Tagish Lake meteorite, *Meteorit. Planet. Sci.*, 41, 407–431.
- Holsapple, K. A. (1993), The scaling of impact processes in planetary sciences, *Ann. Rev. Earth Planet. Sci.*, 21, 333–373.
- Joint Investigation Group (1977), Kirin meteorite shower, *Sci. Sinica*, 20, 502–512.
- Krinov, E. L. (1966), *Giant Meteorites*, 1st English ed., Pergamon Press, New York.
- Levison, H. F. (1996), Comet taxonomy, in *Completing the Inventory of the Solar System*, edited by T. W. Rettig and J. M. Hahn, vol. 107, pp. 173–118.
- Melosh, H. J. (1989), Impact cratering: A geologic process, *Oxford Monographs on Geology and Geophysics No. 11*, Oxford Univ. Press, New York.
- Mukhamednazarov, S. (1999), Observation of a fireball and the fall of the first large meteorite in Turkmenistan, *Astron. Lett.*, 25(2), 117–118.
- Nunez del Prado, H., et al. (2008), The meteorite fall in Carancas, Lake Titicaca Region, Southern Peru: First results, *Lunar Planet. Sci. Conf. XXXIX*, Abstract 2555.
- Petaev, M. I., Y. L. Kisarev, S. A. Mustafin, R. K. Shakurov, A. V. Pavlov, and B. A. Ivanov (1991), Meteorite Sterlitamak—a new crater-forming fall, *22nd Lunar Planet. Sci. Conf.* 1059.
- Petrovic, J. J. (2001), Mechanical properties of meteorites and their constituents, *J. Mater. Sci.*, 36, 1579.
- ReVelle, D. O. (1976), On meteor-generated infrasound, *J. Geophys. Res.*, 81, 1217–1230.
- ReVelle, D. O. (2001a), Bolide fragmentation processes: Single-body modeling versus the catastrophic fragmentation limit, in *Meteoroids 2001 Conf.*, vol. 495, pp. 491–498.
- ReVelle, D. O. (2001b), Bolide dynamics and luminosity modeling: Comparisons between uniform bulk density and porous meteoroid models, in *Meteoroids 2001 Conf.*, vol. 495, pp. 513–517.
- ReVelle, D. O. (2005), Recent advances in bolide entry modeling: A bolide potpourri, *Earth, Moon, Planets*, 97(1–2), 1–35.
- Swinbank, R., and A. A. O'Neill (1994), Stratosphere-Troposphere data assimilation system, *Mon. Weather Rev.*, 122, 686–702.
- Wetherill, G. W., and D. O. ReVelle (1982), Relationships between comets, large meteors, and meteorites, in *Comets*, pp. 297–319, Univ. of Ariz. Press, Tucson, Ariz.
- S. Arrowsmith and D. O. ReVelle, EES-2, Atmospheric, Climate and Environmental Dynamics Group-Meteorological Modeling Team, Los Alamos National Laboratory, P.O. Box 1663, MS D401, Los Alamos, NM 87545, USA.
- P. Brown and E. A. Silber, Department of Physics and Astronomy, University of Western Ontario, London, ON, Canada N6A 3K7. (pbrown@uwo.ca)
- D. Eaton, Department of Geoscience, University of Calgary, 2500 University Drive NW, Calgary, AB, Canada T2N 1N4.
- W. N. Edwards, Department of Earth Sciences, University of Western Ontario, London, ON, Canada N6A 5B7.
- L. E. Jackson Jr., Geological Survey of Canada, Pacific Division, Natural Resources Canada, 16th floor, 625 Robson Street, Vancouver, BC, Canada V6B 5J3.
- G. Tancredi, Dpto Astronomia, Facultad Ciencias, Iguá 4225, 11400 Montevideo, Uruguay.